Stable Yang-Lee zeros in a truncated fugacity series from the net baryon number multiplicity distribution

Kenji Morita[1,2,3,*] and Atsushi Nakamura[4,5]

[1]*Yukawa Institute for Theoretical Physics, Kyoto University, Kyoto 606-8502, Japan*
[2]*Frankfurt Institute for Advanced Studies, Ruth-Moufang-Strasse 1, D-60438 Frankfurt am Main, Germany*
[3]*Institute of Theoretical Physics, University of Wroclaw, PL-50204 Wrocław, Poland*
[4]*Research Center for Nuclear Physics (RCNP), Osaka University, Ibaraki, Osaka 567-0047, Japan*
[5]*Theoretical Research Division, Nishina Center, RIKEN, Wako, Saitama 351-0198, Japan*

(Received 9 June 2015; published 16 December 2015)

We investigate Yang-Lee zeros of grand partition functions as truncated fugacity polynomials of which coefficients are given by the canonical partition functions $Z(T,V,N)$ up to $N \leq N_{\max}$. Such a partition function can be inevitably obtained from the net-baryon number multiplicity distribution in relativistic heavy ion collisions, where the number of the event beyond $N_{\max}$ has insufficient statistics, as well as from canonical approaches in lattice QCD. We use a chiral random matrix model as a solvable model for chiral phase transition in QCD and show that the closest edge of the distribution to the real chemical potential axis is stable against cutting the tail of the multiplicity distribution. A similar behavior is also found in lattice QCD at finite temperature for the Roberge-Weiss transition. In contrast, such a stability is found to be absent in the Skellam distribution which does not have a phase transition. We compare the number of $N_{\max}$ to obtain the stable Yang-Lee zeros with those of critical higher-order cumulants.

DOI: 10.1103/PhysRevD.92.114507 PACS numbers: 12.38.Gc, 12.38.Mh, 25.75.Gz, 25.75.Nq

I. INTRODUCTION

Phase transition in quantum chromodynamics (QCD) is one of the central subjects in high-energy nuclear physics both theoretically and experimentally. First principle lattice QCD (LQCD) calculations have shown that the transition from quark-gluon plasma (QGP) to hadronic matter is of the crossover type at physical quark masses [1] in which order parameters and thermodynamic quantities change smoothly as functions of temperature. At finite baryon density, one expects that the nature of the transition can change. Unfortunately, little is known about the state of matter at high baryon density from LQCD calculations because of the difficulty in numerical simulation at finite baryon chemical potential μ [2,3]. Various approximation methods applied so far seem to work only when $\mu < T$ or a small volume or heavy quark mass region. Nevertheless, effective models which implement relevant symmetries in QCD and large N_c studies have shown that rich phase structure exists in high density [4,5]. In particular, if there is a first-order phase transition at $T = 0$ and large μ, there must be a critical point (CP) at which the first-order phase transition line terminates and the transition becomes second order. The existence of CP is supported by many chiral effective models [6], but its location depends on the detail of the models [7].

Stimulated by these theoretical results, the first beam energy scan program at the Relativistic Heavy Ion Collider (RHIC) has been carried out in search of the CP [8,9]. Since lower colliding energies leave the incident nucleons in the central region, one expects to explore higher baryon density regions at lower energies. There are a number of observables which might have the potential to indicate the transition from QGP to hadronic matter. Among them, event-by-event fluctuations of conserved charges are intimately connected to critical behavior associated with the phase transition [10–13]. Measurements of the net-proton number fluctuations as a proxy of the net-baryon one [14] and net-electric charges have been presented for Au + Au collisions at various energies from $\sqrt{s_{NN}} = 7.7$ to 200 GeV [15–17]. Given the fact that the multiplicity of different particle species is well described by statistical models [18–20], one may regard event-by-event fluctuations of conserved charges as those of the grand canonical ensembles at chemical freeze-out temperature T and baryonic chemical potential μ. Through systematic analyses of the location of (T,μ) corresponding to each colliding systems [20], one can map experimental measurements for property of the matter on the $T-\mu$ plane. Furthermore, recent LQCD results at physical quark masses indicate that the crossover region coincides with the chemical freeze-out at least for $\mu < T$ [21,22]. One may look for remnant of the chiral criticality in the crossover region, originating from the second-order phase transition in the vanishing quark mass [23–25].

Property of the transition can be characterized by behavior of fluctuations of conserved charges as well as an order parameter and its fluctuations [26,27]. In the case

*kmorita@yukawa.kyoto-u.ac.jp

of the chiral phase transition in QCD, the chiral order parameter or quark-antiquark condensate $\langle\bar{q}q\rangle$ couples to quarks carrying the baryon number and the electric charge. Thus, the second-order chiral phase transition in the chiral limit at finite temperature is characterized by not only divergent fluctuation of the order parameter but also higher-order cumulants of the net-baryon number and the net-electric charge [28]. The divergence of the conserved charge fluctuations is governed by the critical exponent of the specific heat α which depends on the universality class QCD belongs to. Although it is not completely determined yet [29,30], recent simulations [31] indicate $O(4)$ in the three dimensions, as conjectured by Pisarski and Wilczek [32]. In this case, the first divergent cumulant appears at the sixth order. At finite but small quark masses, the divergence is replaced by sign change, owing to the property of the universal $O(4)$ scaling function [24,33]. At nonzero net-baryon number density, the divergence at the $2n$th-order cumulants in the chiral limit appears at the nth-order cumulants. The tricritical point in the chiral limit becomes the CP, where the second-order cumulants diverge [26,34,35]. The chemical freeze-out line may locate at lower temperature than the chiral phase boundary [36] such that measured fluctuations might not reflect those at the phase transition [37]. Nevertheless, the existence of the CP is accompanied by the anomalous behavior of the cumulants such as negative third- and fourth-order cumulants around the CP [38–40] and may lead to nonmonotonic behavior of the higher-order cumulants as functions of $\sqrt{s_{NN}}$. Indeed, the measured net-proton number cumulants in [16] seem to follow this expectation, although this is still inconclusive due to uncertainty.

The measurement of the cumulants is based on event-by-event multiplicity distribution. Once the fluctuations are regarded as those of the grand canonical ensemble, the multiplicity distribution can be identified with unnormalized probability distribution.

While the cumulants are expressed by central moments of the probability distribution, it is convenient for theoretical studies to compute them by differentiating the thermodynamic pressure with respect to chemical potentials. Recently, one of the authors (K. M.) investigated the probability distribution of the net-baryon number in models with phase transitions [25,41,42]. It turns out that sufficient information on the tail in the probability distribution is responsible for the critical behavior of the higher-order cumulants and that the remnant of the $O(4)$ criticality can be characterized by a narrower tail than the corresponding reference distribution. In the probability distribution, such information on the phase transition is encoded in the N dependence of the canonical partition function $Z(T,V,N)$.

Since the grand partition function is more straightforward in relativistic quantum field theories where the number of particles are not definite, computations of the canonical partition function are not generally easy. In Ref. [43], Hasenfratz and Toussaint proposed that the canonical partition function, $Z(T,V,N)$, is calculated through the Fourier transformation of the grand canonical partition function, $\mathcal{Z}(T,V,\mu)$, evaluated at pure imaginary μ. The difficulty associated with the complex fermion determinant is replaced by the highly oscillating integral which requires extraordinary numerical precision [41,44,45].

Nevertheless, the probability distribution gives further insights into the property of the system including phase transitions.

In Ref. [46], one of the authors (A. N.) pointed out that one can extract the fugacity parameter $\lambda = e^{\mu/T}$ at the chemical freeze-out and construct $Z(T,V,N)$ for the net-baryon number without any assumption on the property of equilibrium $P(N)$. Furthermore, once $Z(T,V,N)$ is known, one can obtain the grand partition function $\mathcal{Z}(T,V,\mu)$ as a series of fugacity. This enables us to apply Yang-Lee theory for the phase transition [47,48] (for recent reviews, see, e.g., [49,50]), in which zeros of the partition function give information on the thermodynamic property of the system. The zeros of the partition function are distributed on a line in the complex plane of an external parameter and their density grows up with the system volume, then they finally coalesce into the line in the thermodynamic limit. This property leads us, in principle, to obtain the location and order of the phase transition from the distribution of the zeros. Even in the absence of the phase transition, the zeros accumulated on the edge of the distribution exhibit singular behavior. This singularity, known as Yang-Lee edge singularity [51,52], can be regarded as a CP in the complex plane and influences the thermodynamics on the real axis [53].

In both experiments and the canonical approach in LQCD, $Z(T,V,N)$ at large N requires such high statistics that obtained information is limited to some finite N; thus, one has to truncate the fugacity polynomial there in reconstructing the grand partition function (see [54,55] for recent LQCD calculations). It is not *a priori* clear whether one can obtain the correct information on the phase transition from such a truncated partition function. The purpose of this paper is to clarify this point. We employ a solvable model for the chiral phase transition in QCD. We present the Yang-Lee zeros in a chiral random matrix model, both for the exact grand partition function and for the reconstructed one as a truncated fugacity series with the canonical partition function being the coefficients. We discuss effects of the truncation on the distribution of the Yang-Lee zeros and compare it with the spurious zeros of the Skellam partition function, originated from the truncation.

In the next section, we briefly summarize the general relation among the probability distribution, partition functions, and Yang-Lee zeros. A chiral random matrix model and its Yang-Lee zeros are presented in Sec. III. We demonstrate differences of the truncation effects on the

Yang-Lee zeros between the models with and without phase transition in Sec. IV. Implications for heavy ion experiments are discussed in Sec. V. Section VI is devoted to concluding remarks. Detailed expressions for partition functions in the chiral random matrix model are given in Appendix A.

II. GENERAL FRAMEWORK

We start from the experimentally measured data of net-baryon number multiplicity distribution $\mathcal{P}(N)$, where N is the net-baryon number. In real experiments one measures the net-proton number $\Delta N_p = N_p - N_{\bar{p}}$. In principle, one can reconstruct $\mathcal{P}(N)$ from $\mathcal{P}(\Delta N_p)$, $\mathcal{P}(N_p)$, and $\mathcal{P}(N_{\bar{p}})$ [56]. In this study we entirely assume the isospin invariance and regard $\mathcal{P}(\Delta N_p)$ as a proxy of $\mathcal{P}(N)$. The shape of the distribution depends on the colliding energies, centrality, etc. The net-baryon number can take any value as long as it can be packed within the system volume. Owing to limited statistics, however, we do not observe such states that have too large N far from its mean value M. Thus, we define the possible minimum and maximum of $N_{\rm min}$ and $N_{\rm max}$ as

$$\mathcal{P}(N < N_{\rm min}) = 0$$
$$\mathcal{P}(N > N_{\rm max}) = 0. \tag{1}$$

In thermal equilibrium, probability distribution of the net-baryon number in the grand canonical ensemble reads, for the fugacity factor $\lambda = e^{\mu/T}$,

$$P(T, V, N, \mu) = \frac{Z(T, V, N)\lambda^N}{\mathcal{Z}(T, V, \mu)}, \tag{2}$$

where $\mathcal{Z}(T, V, \mu)$ is the grand partition function,

$$\mathcal{Z}(T, V, \mu) = \mathrm{Tr}[e^{-(\hat{H}-\mu\hat{N})/T}], \tag{3}$$

and $Z(T, V, N)$ is the canonical partition function,

$$Z(T, V, N) = \mathrm{Tr}[e^{-\hat{H}/T}\delta_{\hat{N},N}]. \tag{4}$$

Assuming the measured multiplicity distribution is the equilibrium one, one finds N dependence of $\mathcal{P}(N)$ comes from $Z(T, V, N)\lambda^N$. Using the charge-conjugate symmetry $Z(T, V, -N) = Z(T, V, N)$, one can determine λ from $\mathcal{P}(N)$ and obtain the canonical partition function [46]

$$Z(T, V, N) = \mathcal{P}(N)\lambda^{-N}. \tag{5}$$

Because of the limited range of N (1), the canonical partition function (4) can be obtained for $N \in [\max(0, N_{\rm min}), N_{\rm max}]$. For the energy scan range in RHIC experiments, $N_{\rm min} < 0$, i.e., there are a few events in which more antiprotons are observed than protons, except for $\sqrt{s_{NN}} = 7.7$ GeV where $N_{\rm min} = 1$ [16]. Note that we need only $N \geq 0$ thanks to the charge conjugate symmetry. Thus, in most cases, one can extract the canonical partition function for $-N_{\rm max} \leq N \leq N_{\rm max}$.

This limitation in N also applies to theoretical approaches such as model studies [25,41,42] and lattice simulations [54,55]. In the former, the canonical partition functions have been calculated using a projection formula,

$$Z(T, V, N) = \frac{1}{2\pi i}\oint d\lambda \frac{\mathcal{Z}(T, V, \lambda)}{\lambda^{N+1}}, \tag{6}$$

where integration contour C in the complex λ plane can be arbitrary, but it is convenient to take the unit circle $\lambda = e^{i\theta}$. Then the formula becomes

$$Z(T, V, N) = \frac{1}{2\pi}\int_{-\pi}^{\pi} d\theta \cos(N\theta)\mathcal{Z}(T, V, \theta), \tag{7}$$

where θ is related to an imaginary chemical potential $-i\mu/T$. In Refs. [25,41,42], the thermodynamic potential $\Omega = -pV$ in Landau theory [41] and in a chiral quark-meson model [25,42] was used through $\mathcal{Z}(T, V, \theta) = e^{-\Omega(T,\theta)/T}$. Owing to the rapid oscillation in large N, it turned out that the numerical integration in double precision works up to $P(N) \simeq 10^{-12}$.

In lattice QCD simulations, two approaches can provide the canonical partition functions, i.e., (i) the fugacity expansion of the fermion determinant [57] and (ii) the Hasenfratz and Toussaint method [43]. In the fugacity expansion, we must diagonalize a matrix whose rank is proportional to the lattice spacial volume. This requires large computational resources and currently one cannot go to simulations on large lattices. In the method (ii), as N increases, more accuracy is needed, and consequently N cannot become very large.

Once the canonical partition function $Z(T, V, N)$ is obtained, one can also construct a *truncated* grand canonical partition function as a series in λ:

$$\mathcal{Z}^{\rm tr}(T, V, \lambda; N_{\rm max}) = \sum_{N=-N_{\rm max}}^{N_{\rm max}} Z(T, V, N)\lambda^N. \tag{8}$$

Owing to the truncation of the series at $N = -N_{\rm max}$ and $N_{\rm max}$, this partition function is an approximation of the exact partition function which could be obtained if one takes $N_{\rm max} = N^*$ with N^* being the number of net-baryon fulfilling the system volume [47]. For lattice QCD at finite temperature with $N_s^3 \times N_t$ lattice, $N^* = 2N_s^3$ [57].[1] Thus, one needs to establish the relations of physical quantities obtained from the truncated partition function (8) with those from the exact partition function. As seen in the

[1] In Ref. [57], N^* was derived for the quark fugacity series as $N_q^* = 2N_c N_s^3$.

summation running from $-N_{\max}$, relativistic partition functions contain negative powers of λ. The suppression of a high-N contribution to $\mathcal{Z}$ cannot be realized by a small λ. One needs to know the large-N behavior in $Z(T,V,N)$.

Similar studies on higher-order cumulants of the net-baryon number have been carried out in Ref. [42], in which sufficiently large $N_{\max}$ depending on the order of the cumulants is shown to be necessary to obtain a correct value of the cumulants. In this paper, we focus on Yang-Lee zeros for the baryon chemical potential.

The zeros of the partition function in a complex chemical potential plane can be obtained by solving an equation,

$$\mathcal{Z}(T,V,\mu)=0, \tag{9}$$

for complex μ. Owing to the negative powers of the fugacity, the equation is a polynomial one in λ with order $2N^*$. For the truncated partition function $\mathcal{Z}^{\rm tr}$, one needs to solve

$$\mathcal{Z}^{\rm tr}(T,V,\mu;N_{\max})=0, \tag{10}$$

of which the order of the polynomial is $2N_{\max}$.

In the exact case, the roots have both real and imaginary parts whose distribution in the complex chemical potential plane is expected to form a line that crosses the real axis at the transition point in the thermodynamic limit. The behavior of the distribution depends on the nature of the phase transition. In Ref. [58], the behavior of the Yang-Lee zeros around the CP was studied by using a chiral random matrix model. The singularity associated with the CP appears as a branch point in the complex μ plane, and its property is shown to be connected with the universality. In lattice QCD, the phase transition between the different $Z(N_c)$ sector in the deconfined phase, the Roberge-Weiss phase transition, has been recently analyzed from the viewpoint of the Yang-Lee zeros [55]. In this work, we use a chiral random matrix model similar to that used in Ref. [58] but with an extension to periodic property in the imaginary chemical potential as it is necessary to have an integer net-baryon number.

The partition function is written as a polynomial in $\lambda=e^{\mu/T}$. Since a complex root λ_1 is accompanied with its conjugate $\bar{\lambda}_1$ and the charge conjugate symmetry implies $1/\lambda_1$ and $1/\bar{\lambda}_1$ are also roots, only the roots located in the first quadrant of the complex μ plane are independent. In practice, it is convenient to use a Joukowski transformation $\omega=\lambda+1/\lambda(=2\cosh\beta\mu)$ and reorganize the series in terms of ω to reduce the number of roots that need to be located. Using a property of the Chebychev polynomial $T_n(\cosh x)=\cosh(nx)$, one finds

$$\lambda^N+\frac{1}{\lambda^N}=2\cosh(\beta\mu N)=2T_N(\cosh\beta\mu)=2T_N(\omega/2). \tag{11}$$

Then Eq. (8) reduces to a series expression containing only positive powers. After expanding the Chebychev polynomial by Eq. (A7), one finds

$$\mathcal{Z}^{\rm tr}(T,V,\omega;N_{\max})=Z(T,V,N=0)+\sum_{n=1}^{N_{\max}}nZ(T,V,n)\times\sum_{k=0}^{[n/2]}(-1)^k\frac{(n-k-1)!}{k!(n-2k)!}\omega^{n-2k}. \tag{12}$$

This formula could be also useful to compare a relativistic system with nonrelativistic ones. The roots of ω space are easily converted into those in the λ and μ plane as

$$\frac{\mu}{T}=\pm\cosh^{-1}\frac{\omega}{2}. \tag{13}$$

Taking both signs, one can finds all the roots in the complex μ and λ plane.

III. CHIRAL RANDOM MATRIX MODEL

In this section, we introduce a chiral random matrix model which is an effective model for the spontaneous chiral symmetry breaking in QCD. Since this model is analytically solvable in the chiral and thermodynamic limit [59] and the analytic expression for the partition function in finite volume is known [58], we find this model to be the most suitable one for the present purpose. An apparent shortcoming of the model as applied to the net-baryon number probability distribution is its lack of periodicity in the imaginary chemical potential, which is a consequence of $U(1)_B$ symmetry. Thus, we first extend the model to exhibit the appropriate periodicity and the phase structure in the imaginary baryon chemical potential.

In QCD, the partition function has a periodicity $2\pi/N_c$ in the imaginary quark chemical potential $\theta_q=\theta/3$, thus 2π in the imaginary baryon chemical potential. LQCD simulations have shown that there is no phase transition in the imaginary baryon chemical potential at temperatures below the chiral crossover temperature, and thermodynamic quantities smoothly behave as $\sim\cos\theta$ [60–62]. This fact combined with Eq. (7) implies that the phase transition at large baryon number density is encoded in higher Fourier coefficients of the smoothly oscillating function.

A. Partition function and thermodynamics

We start with a partition function of the chiral random matrix model with N_s sites given in [59]

$$\mathcal{Z}_{\rm RM}=\int\mathcal{D}X\exp\left(-\frac{N_s}{\sigma^2}{\rm Tr}XX^\dagger\right)\det{}^{N_f}(D+m), \tag{14}$$

where σ denotes the variance of the random matrix X which has $N_s \times N_s$ dimension and D is the $2N_s \times 2N_s$ matrix approximating the Dirac operator. At $T = \mu = m = 0$, σ is the only dimensionful parameter. We use it as a unit of mass in the model and put $\sigma = 1$ in the expressions below.

The Dirac operator takes the form

$$D = \begin{pmatrix} 0 & iX + iC \\ iX^\dagger + iC & 0 \end{pmatrix}. \tag{15}$$

The matrix C describes the effect of temperature and chemical potential. In Ref. [59], it was chosen as

$$C_k = a\pi T + \frac{b\mu}{iN_c} \tag{16}$$

for one half of the eigenvalues and

$$C_k = -a\pi T + \frac{b\mu}{iN_c} \tag{17}$$

for the other half,[2] with a and b being the dimensionless parameters.

The linear ansatz for the matrix C (16)–(17) accounts for the fact that these are the two smallest Matsubara frequencies $\pm\pi T$. This model does not have any thermal distribution which gives the fugacity factor $e^{\mu/T}$ nor any periodicity in the imaginary chemical potential since it appears as a result of summation over the Matsubara frequencies. In order to make the partition function periodic, we perform the following replacement,

$$\frac{b}{N_c}\mu + i\pi aT = \pi aT\left(i + \frac{b}{a\pi N_c}\frac{\mu}{T}\right) \tag{18}$$

$$\to \pi aT\left(i + \frac{b}{a\pi N_c} 2\sinh\frac{\mu}{2T}\right), \tag{19}$$

which gives a periodicity $2\pi T$ in μ_I to the partition function. Compared to the original linear ansatz, this replacement does not change anything at $\mu = 0$ but alters the phase structure at $\mu > 2T$.

The phase structure of the model is easily evaluated by taking $N_s \to \infty$ limit. Introducing an auxiliary $N_f \times N_f$ complex matrix field ϕ and performing the Gaussian integration with respect to X, one obtains the partition function [63]

$$\mathcal{Z}_{\rm RM} = \int \mathcal{D}\phi \exp[-N_s\Omega(\phi)], \tag{20}$$

where $\Omega(\phi)$ stands for the effective potential. Then the partition function can be determined by the minimum of the potential, which is evaluated at the saddle point ϕ_0 of the integrand,

$$\left.\frac{\partial\Omega(\phi)}{\partial\phi}\right|_{\phi=\phi_0} = 0, \tag{21}$$

and

$$\lim_{N_s\to\infty}\frac{1}{N_s}\ln\mathcal{Z}_{\rm RM} = -\min_{\phi}\Omega(\phi). \tag{22}$$

The saddle point ϕ_0 is related to the chiral condensate through

$$\langle\bar\psi\psi\rangle = \frac{1}{N_f V_4}\frac{\partial\ln\mathcal{Z}_{\rm RM}}{\partial m}, \tag{23}$$

$$= \frac{1}{N_f V_4}\frac{N_s}{\sigma} 2{\rm ReTr}\phi_0, \tag{24}$$

where the four-dimensional volume V_4 corresponds to N_s such that N_s represents the typical number of the instanton (or anti-instanton) in V_4. For real m, one expects ϕ_0 is a real matrix proportional to the unit matrix. Therefore, the saddle point can be obtained by solving (21) for the potential

$$\Omega(\phi)/N_f = \phi^2 - \frac{1}{2}\ln\left\{\left[(\phi+m)^2 - \tilde T^2\left(A\sinh\frac{\mu}{2T} + i\right)^2\right] \times \left[(\phi+m)^2 - \tilde T^2\left(A\sinh\frac{\mu}{2T} - i\right)^2\right]\right\}, \tag{25}$$

where

$$\tilde T \equiv \pi aT \tag{26}$$

and

$$A \equiv \frac{2b}{a\pi N_c}. \tag{27}$$

In the chiral limit $m = 0$, one finds that $\phi_0 = 1$ at $T = \mu = 0$ and a second-order phase transition occurs at $T = 1/(\pi a)$ and $\mu = 0$, where ϕ_0 continuously approaches zero. Thus, ϕ_0 can be regarded as an order parameter of the chiral phase transition.

The parameters in the model—σ, a, and b—are determined as follows. The only dimensionful parameter σ is estimated to be $\sigma \sim 100$ MeV through Eq. (24) by putting $\langle\bar\psi\psi\rangle \sim 2$ fm^{-3} at $T = \mu = 0$. Since $T_c = 1/(\pi a)$ at $\mu = 0$, putting $T_c = 160$ MeV yields $a = 0.2$. The remaining parameter b connects the model to the density scale.

[2]Note that μ is the chemical potential of the baryon number; thus, μ/N_c stands for that of the quark number.

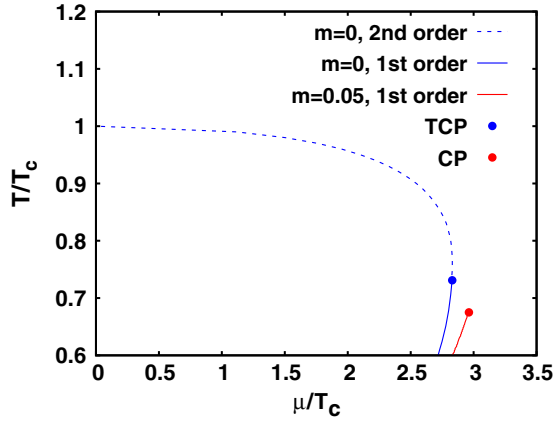

FIG. 1 (color online). Phase diagram of the chiral random matrix model with periodicity in the imaginary baryonic chemical potential.

With the linear ansatz for C (16)–(17), one finds the first-order phase transition at $T = 0$ and $b\mu/N_c = 0.528$. We follow the choice of Ref. [59] and put $b = 0.13$, corresponding to the first-order transition point at $\mu_c \simeq 1200$ MeV, though we do not have the same phase diagram as Ref. [59] owing to the implementation of the periodicity (16)–(17).

Figure 1 shows the phase diagram of the modified random matrix model (25) in the chiral limit and in the presence of a small explicit symmetry breaking, $m = 0.05$, respectively. In the chiral limit, the second-order line continues with decreasing temperature down to $T > T_3$ and $\mu < \mu_3$, where $T_3 \simeq 0.731T_c$ and $\mu_3 \simeq 4.504$ is the location of the tricritical point (TCP). Below T_3, there is the first-order phase transition line. At finite quark mass, the second-order line is replaced by smooth crossover and TCP becomes CP with slightly decreased temperature and increased chemical potential, $T_{\rm CP} = 0.675T_c$ and $\mu_{\rm CP} = 4.72$, respectively. While these structures are the same as those in Refs. [58,59], the apparent singularity at $T = 0$ in the periodic parametrization significantly modifies the phase boundary at low temperature. We stress that our purpose in this paper is to explore the property of partition function zeros rather than determining the phase structure.

With the parameter set for a, b, and σ, we find that this form also gives reasonable thermodynamic quantities at the imaginary chemical potential.[3] Figure 2 displays the behavior of the order parameter ϕ_0 in the imaginary baryonic chemical potential $\theta = \mu_I/T$. One sees that our parametrization (19) gives the correct periodicity 2π and the expected temperature dependence such as a larger amplitude at higher temperature below T_c [64,65]. Owing to the lack of a $Z(3)$ sector such as the Polyakov loop background, this model does not exhibit the Roberge-Weiss phase transition [66] at high T.

At finite N_s, the partition function can be expressed as [58]

$$\mathcal{Z}_{\rm RM} = \sum_{k_1,k_2=0}^{N_s/2} \binom{N_s/2}{k_1}\binom{N_s/2}{k_2}(N_s-k_1-k_2)! \times {}_1F_1(k_1+k_2-N_s;1;-m^2N_s)(-N_s\tilde{T}^2)^{k_1+k_2} \times \left(i + A\sinh\frac{\mu}{2T}\right)^{2k_1}\left(i - A\sinh\frac{\mu}{2T}\right)^{2k_2}, \quad (28)$$

where an irrelevant constant factor is ignored and ${}_1F_1(a,b;x)$ denotes the confluent hypergeometric function. One may directly obtain zeros of this partition function, but one needs to expand $\mathcal{Z}$ in a series of the fugacity λ to examine the effects of tails in the probability distribution function. We put the details in Appendix A and write down only the result for the canonical partition function, for $\delta \equiv |k_1 - k_2|$,

$$Z(T,N_s,N) = \sum_{k_1,k_2=0}^{N_s/2} \binom{N_s/2}{k_1}\binom{N_s/2}{k_2}(N_s-k_1-k_2)!\,{}_1F_1(k_1+k_2-N_s;1;-m^2N_s)(-N_s\tilde{T}^2A^2/4)^{k_1+k_2} \times \begin{cases} \sum_{k_3=0}^{k_1+k_2}\binom{k_1+k_2}{k_3}\left[\frac{2(2-A^2)}{A^2}\right]^{k_1+k_2-k_3}\binom{k_3}{\frac{k_3-N}{2}} & k_1 = k_2 \\ \delta\sum_{k_3=0}^{\delta}\left(-\frac{16}{A^2}\right)^{k_3}\frac{(\delta+k_3-1)!}{(\delta-k_3)!(2k_3)!}\sum_{k_4=0}^{k_1+k_2-k_3}\binom{k_1+k_2-k_3}{k_4}\left[\frac{2(2-A^2)}{A^2}\right]^{k_1+k_2-k_3-k_4}\binom{k_4}{\frac{k_4-N}{2}} & k_1 \neq k_2. \end{cases} \quad (29)$$

B. Phase boundary and Yang-Lee zeros

We compute the Yang-Lee zeros for the truncated partition function (12) with the canonical partition function of the chiral random matrix model (29). Taking $N_{\rm max} = N_s$ in Eq. (12), one recovers the exact grand partition function (28). The computation of the zeros requires special care with the numerical digits as cautioned in the literature

[3]Note that in Refs. [58,59] the coefficients in the temperature and chemical potential are absorbed into T and μ. While the qualitative phase structure does not depend on the parameters in the linear ansatz, it does so when one employs the periodic parametrization (19).

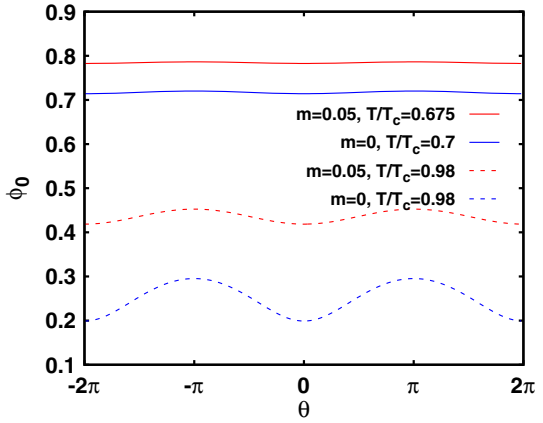

FIG. 2 (color online). Behavior of the order parameter ϕ_0 of a periodic chiral random matrix model in imaginary chemical potential $\theta = \mu_I/T$ at $\mu_R = 0$.

[46,67]. We perform the calculations in 50–300 digits utilizing the FMLIB package [68] in FORTRAN 90.

Figure 3 shows the distribution of the Yang-Lee zero of the periodic chiral random matrix model in the complex ω plane for $m = 0$ and at $T/T_c = 0.99$. The distribution of the zeros is symmetric with respect to the horizontal axis because the partition function is an even-order polynomial of ω and the root has its complex conjugate. The solid line in Fig. 3 stands for the Stokes boundary, which can be regarded as an extension of the phase boundary to a complex chemical potential plane. In the thermodynamic limit $N_s \to \infty$, it satisfies

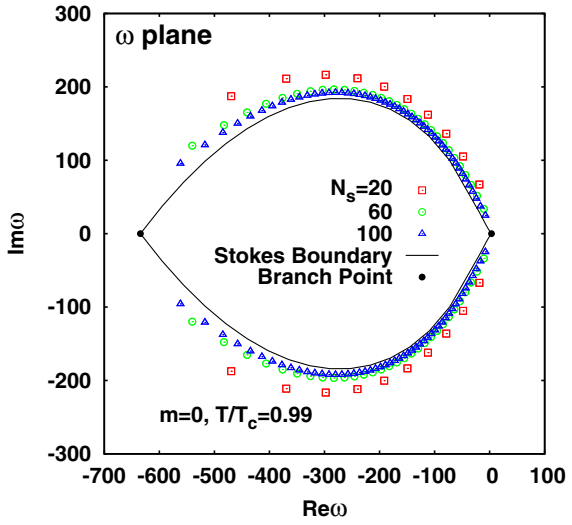

FIG. 3 (color online). Yang-Lee zeros of the periodic random matrix model in the complex ω plane for $m = 0$ at $T/T_c = 0.99$. Open symbols stand for the zeros in different N_s and the solid line indicates the Stokes boundary. The branch point is denoted by closed circles.

$$\mathrm{Re}\left(\left.\frac{\partial^2\Omega(\phi)}{\partial\phi^2}\right|_{\phi=\phi_0}\right) > 0, \tag{30}$$

$$\mathrm{Re}\Omega(\phi = \phi_{0,1}) = \mathrm{Re}\Omega(\phi = \phi_{0,2}), \tag{31}$$

where the first condition ensures the well-defined partition function at the saddle point of the integrand in Eq. (20) and the second condition denotes the continuity of the real part of the pressure at the boundary [58]. $\phi_{0,1}$ and $\phi_{0,2}$ stand for two out of five solutions of the gap equation $\partial\Omega/\partial\phi = 0$ and give the minimum of $\mathrm{Re}\Omega$ in both sides of the boundary, respectively. The density of the zeros increases with N_s and turns into the cut which constitutes the Stokes boundary in the thermodynamic limit. This is clearly seen in Fig. 3. There are two branch points located on the real axis. Since $\omega = \lambda + 1/\lambda > 0$ for real μ, the one at $\mathrm{Re}\omega = \omega_c = 3.4 > 0$ corresponds to the second-order phase transition point in real μ, while the other one, $\mathrm{Re}\omega = -634.4$, is located on the line $\mathrm{Im}\mu/T = \pi$. The Stokes boundary exhibits a closed curve, reflecting the periodicity in imaginary μ and existence of the phase boundary at the real μ axis and $\mathrm{Im}\mu/T = \pi$.

The phase structure can be more intuitively understood by going to the complex μ plane. Figure 4 (left) displays the distribution of the same Yang-Lee zeros as in Fig. 3, but the zeros in $\mathrm{Re}\mu < 0$ are omitted since their locations are trivial according to the charge conjugate symmetry $\mu \to -\mu$. The branching point on the horizontal axis indicates the second-order phase transition point. The Stokes boundary extends to both direction in imaginary μ and ends up at the other branch point. Note that the branch points at $\mathrm{Im}\mu/T = -\pi$ and π are essentially the same because of the periodicity. We refer to [69,70] for behavior of the order parameter in complex μ plane and related topics. The zeros distribute along the boundary and becomes more dense for large N_s, but distance to the real axis is not so close for these values of N_s. The behavior of the density of the zeros is related to a property of the thermodynamic potential which can be described by an analogy to electrostatics [58]. In this case, $\mathrm{Re}\Omega$ can be regarded as the electrostatic potential on the $\mathrm{Re}\mu/T - \mathrm{Im}\mu/T$ plane and the normal component of the electric field $\mathbf{E} = -\nabla(\mathrm{Re}\Omega)$ to the Stokes boundary has a discontinuity proportional to the density of the zeros. We confirmed that in this model these discontinuities at large $\mathrm{Re}\mu$, where the zeros are dense, are much larger than those at small μ, as expected. Although the density of the zeros far from the branching point is a model-dependent feature dependent on the shape of the Stokes boundary, it is governed by the universality near the branch point on the real axis, as pointed out in Ref. [58].

The effects of the finite but small quark mass can be seen in the right panel of Fig. 4 where the distribution of Yang-Lee zeros for $m = 0.05$ at the same temperature is displayed. Because of the explicit chiral symmetry breaking, the phase transition becomes a crossover such that the

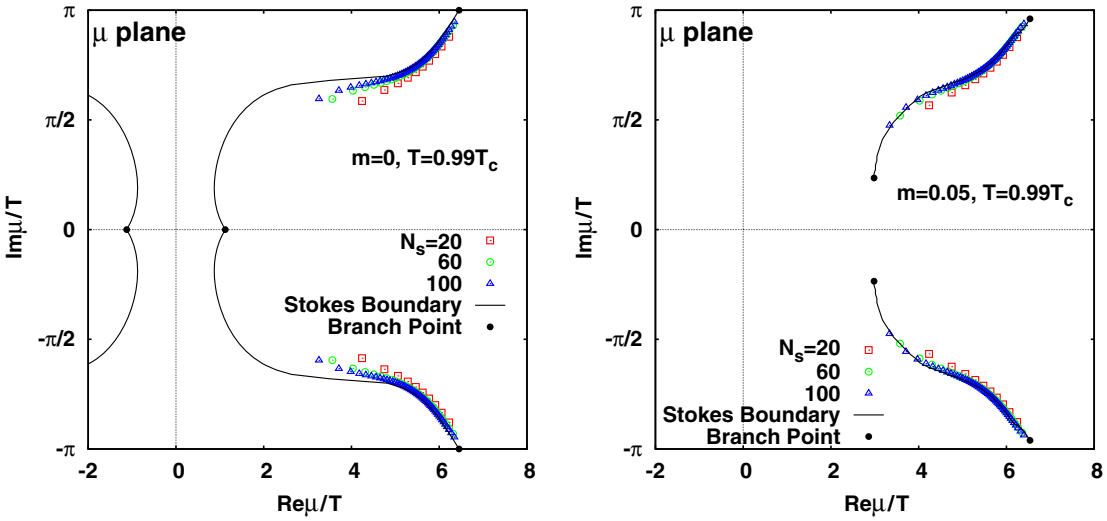

FIG. 4 (color online). Yang-Lee zeros of the periodic random matrix model in complex μ plane. The left panel corresponds to the case of Fig. 3. Right panel shows the case with a finite but small quark mass, $m = 0.05$ at the same temperature.

branch point on the real axis moves above it. As a result, there are two branch points of which are complex conjugate each other. The same thing occurs also to the branch point at $\mathrm{Im}\mu/T = \pm\pi$. Here we emphasize that these complex singularities are, albeit unphysical, indicating the existence of a chiral phase transition in the chiral limit. These are also known as Yang-Lee edge singularities [52]. The critical point at finite density (See Fig. 1) is realized by the coalescence of the branch points close to the real μ axis when the temperature is decreased [53]. As seen in Fig. 4 (right), the Yang-Lee zeros are fairly on the boundary line and exhibit expected behaviors.

IV. YANG-LEE ZEROS FROM TRUNCATED PARTITION FUNCTIONS

As described in Sec. II, the connection of net-baryon number multiplicity distribution (2) with the reconstructed grand partition function (8) could potentially enable us to extract the Yang-Lee zeros from experimental data. Since the results presented in the previous section correspond to $N_{\mathrm{max}} = N^*$, i.e., no information on the exact partition function is lost, we need to evaluate whether one can obtain the correct distribution of the Yang-Lee zeros when the fugacity expansion is truncated. Furthermore, even if one starts from a partition function which does not exhibit any phase transition, such as an ideal Boltzmann gas, the truncation produces the zeros of the partition function because it is a polynomial of order N_{max}. In this section we investigate in detail the effects of the truncation on the distribution of the Yang-Lee zeros.

A. Random matrix model

Figures 5 and 6 display the distribution of the Yang-Lee zeros from the truncated partition function of the periodic chiral random matrix model for various N_{max} and $m = 0.05$.[4] Hereafter, we set $N_s = 60$. We confirm the following results do not depend on the specific choice of N_s. We plot only the first quadrant in the complex μ plane according to the symmetry structure of the distribution.

The left panel in Fig. 5 shows the case of $T = T_c$, at which the transition is of the crossover type, as seen in the branch point at $(\mathrm{Re}\mu/T, \mathrm{Im}\mu/T) \simeq (3, \pi/4)$. For $N_{\mathrm{max}} = 60 = N_s$, the zeros are located on the Stokes boundary (dashed line). Reducing N_{max} by one, i.e., removing $Z(N = 60)$ from the series, one sees a drastic change in the distribution. The distribution of the zeros at large $\mathrm{Re}\mu$ and $\mathrm{Im}\mu$ splits into the two lines, but the rest of the zeros remain unchanged. Further reduction of N_{max} substantially modifies the distribution such that the splitting occurs closer to the edge that is closer to the real μ axis. Nevertheless, up to $N_{\mathrm{max}} = 21$, the edge of the distribution which is the closest Yang-Lee zero to the real μ axis remains the same. Beyond $N_{\mathrm{max}} = 20$, the distribution no longer holds the information on the exact Yang-Lee zeros; thus, the apparent relation to the phase boundary is lost.

The behavior with respect to changing N_{max} does not depend on temperature or corresponding phase transition. In the right panel of Fig. 5, we plot the result of the same analysis for $T = T_{\mathrm{CP}} = 0.675T_c$, where the branch point appears on the real axis, indicating the critical point. Reflecting the location of the branch point, the edge of the distribution also becomes closer to the real axis compared to the crossover case. The edge is stable against decreasing N_{max} down to $N_{\mathrm{max}} = 19$, then it starts to deviate slowly when decreased further. This is also true in the case of the first-order phase transition ($T = 0.6T_c$)

[4]Note that T_c is defined for $m = 0$. Thus, it is slightly lower than the chiral crossover temperature for $m = 0.05$.

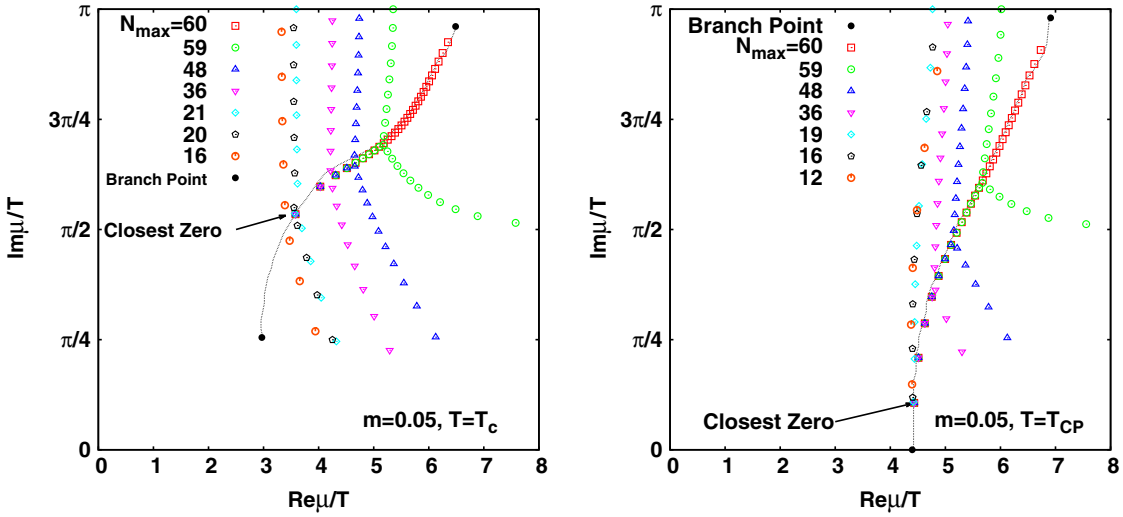

FIG. 5 (color online). Distribution of the Yang-Lee zeros from the truncated partition function of the periodic chiral random matrix model for $m = 0.05$. Left and right panels stand for $T = T_c$ and $T = T_{\mathrm{CP}}$, respectively.

depicted in Fig. 6. The branch point is hidden in the unphysical Riemann sheets [70], and the edge is very close to the real axis.

We also note that there is always a zero at $\mathrm{Im}\mu/T = \pi$ when N_{max} is odd. These zeros look special since they correspond to the negative real axis in the complex λ and ω plane. However, this is a mathematical consequence because in this case the truncated partition function (12) is an odd-order polynomial; thus, it has at least one real root. As seen in Figs. 5 and 6, it becomes the edge of one of the lines bifurcating from the exact Yang-Lee zeros.

These results indicate the stability of the edge does not depend on the detail of the phase structure, although the location of the edge seems to be connected with the shape of the Stokes boundary which is model dependent through the μ dependence of the partition function. In particular, the present results are obtained by employing the periodicity (19) in the random matrix model which does not correctly take into account degrees of freedom with baryon charges [59]. We note that this modification causes unphysical behavior in thermodynamics, such as negative $Z(T, V, N)$ at some small N at low T, which presumably reflects the unusual curvature of the phase boundary in Fig. 1. Therefore, we note that the shape of the distribution itself might not be relevant for realistic situations. Nevertheless, below we shall see that the stability of the edge is specific to the case with a phase transition.

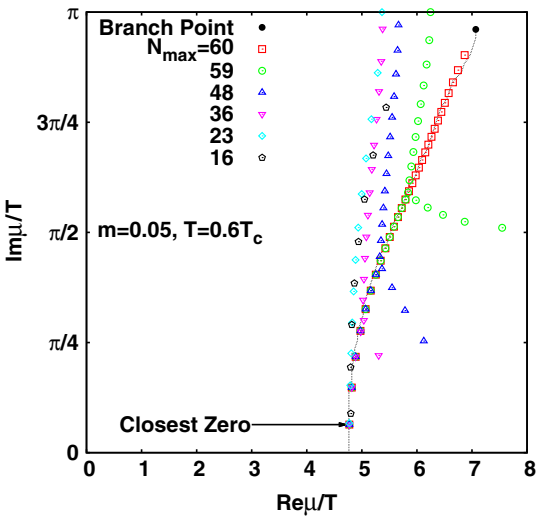

FIG. 6 (color online). Same as Fig. 5, but for $T = 0.6T_c$.

B. Lattice QCD

Figure 7 displays the distribution of the Yang-Lee zeros above T_c calculated in the lattice QCD simulation via the canonical method [54]. While calculations in the confinement phase are still numerically difficult such that we do not see clear indications of a phase transition at low T, the Roberge-Weiss (RW) transition [66] provides us a well-defined phase transition in the high-temperature quark-gluon plasma phase at an imaginary chemical potential. In this figure, the data are calculated on $8^3 \times 4$ lattices and $\beta = 1.89$ which corresponds to $T/T_c \simeq 1.94$. A more detailed analysis in lattice QCD with different lattice setups can be found in Ref. [55]. Since quark mass is heavy, the calculation is not relevant for the chiral phase transition. The RW transition is regarded as a transition from one $Z(3)$ sector to another one when single quarks can be excited because of deconfinement and are known to exhibit a first-order phase transition at $\mathrm{Im}\mu_q/T = \pm\pi/3$. In terms of the baryon chemical potential, the transition lines reduce to $\mathrm{Im}\mu/T = \pm\pi$, which is shown as a dotted line in Fig. 7. A brief explanation of the Roberge-Weiss phase boundary can be found in Appendix B. Since it is hard to compute $Z(N)$ near $N = N^*$, the canonical approach in lattice QCD lacks

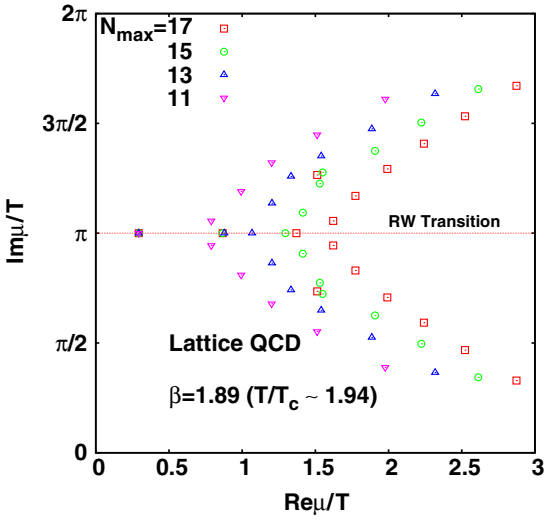

FIG. 7 (color online). Distribution of Yang-Lee zeros for a lattice QCD data [54].

the large-N contribution when one constructs the truncated partition function (12). One sees that in Fig. 7 the behavior of the distribution of the Yang-Lee zeros against changing $N_{\max}$ is similar to that of the random matrix model, despite the completely different origin of the phase transition. Therefore, we expect the similar splitting behavior of the distribution also appearing in Refs. [46,55] is also due to the truncation effect. Indeed, the N_s and $N_{\max}$ dependence of the Yang-Lee zero shown in Ref. [55] agrees with the truncation effects discussed here. We expect that the bifurcation of the zero starts at large Reμ by improving the fugacity expansion, but one needs to take $N_{\max} = N^*$ to completely produce the Yang-Lee zero along the transition line. In the RW transition where the transition point occurs at $\mathrm{Im}\mu/T = \pm\pi$, the edge of the distribution is the closest zero to the imaginary axis. One sees that this point is also stable against changing $N_{\max}$. This fact suggests that the stability of the edge is not specific to the random matrix model or chiral phase transition but might be a general property of the distribution when the partition function is truncated.

C. Skellam distribution

Finally, we examine a model without phase transition in order to check whether the stability of the edge is specific to the phase transition. We employ the Skellam distribution [71] for which the probability distribution of the net-baryon number N is given by

$$P^S(N) = \left(\frac{N_B}{N_{\bar{B}}}\right)^{N/2} I_N(2\sqrt{N_B N_{\bar{B}}}) e^{-(N_B+N_{\bar{B}})}, \qquad (32)$$

where N_B and $N_{\bar{B}}$ denote the thermal averages of the numbers of baryons and antibaryons, respectively. The mean M and variance σ^2 of the distribution are given by $M = N_B - N_{\bar{B}}$ and $\sigma^2 = N_B + N_{\bar{B}}$, respectively. For $N_B = N_{\bar{B}}$, the distribution becomes symmetric and the argument of the modified Bessel function $I_N(x)$ is reduced to $2N_B = \sigma^2$. This distribution can be derived from the noninteracting Boltzmann gas [18]; thus, the canonical and grand canonical partition functions read

$$Z(N) = I_N(\sigma^2) \qquad (33)$$

$$\mathcal{Z}(\lambda) = \exp\left[\frac{\sigma^2}{2}\left(\lambda + \frac{1}{\lambda}\right)\right], \qquad (34)$$

where the temperature and volume dependence is encoded in σ^2. Obviously the grand partition function (34) does not have any roots; thus, no phase transition exists. When one constructs the truncated grand partition function (8) from the canonical partition function (33), however, there exist complex roots. Consequently, one might see these spurious zeros even if the system does not have any phase transition when one constructs the partition function through the fugacity expansion.

Here we investigate such spurious zeros from the Skellam partition function (33) such that it has the same variance with the random matrix model at $N_s = 60$, $T = T_c$, and $m = 0.05$ for which the distribution of the Yang-Lee zeros is displayed in Fig. 5. Since the information on the phase transition is encoded in the tail of the probability distribution $P(N)$, the Skellam distribution with the same variance serves as a useful reference distribution [25]. The probability distribution of the random matrix model and corresponding Skellam distribution are shown in Fig. 8 (left). Both distributions almost agree for small N, according to the same σ^2, but the deviation appears in the tail of the distribution with tiny probability.

Figure 8 (right) shows the distribution of zeros of the truncated partition function for the Skellam distribution with $\sigma^2 = 0.365$. Except for a splitting of the distribution for $N_{\max} \geq 70$ which is similar to those in the random matrix model, the distributions consist almost parallel lines moving to large real μ direction as $N_{\max}$ increases. This behavior reflects the fact that all the zeros go away to infinity as $N_{\max} \to \infty$ since the exact grand partition function does not have roots. Remarkably, the edges of the distributions also move together with the rest of the zeros, in contrast to the random matrix model and lattice QCD. Furthermore, one notes that the distributions for $N_{\max} \leq 20$ in the random matrix model, shown in Fig. 5, resemble those from the Skellam distribution. This observation indicates that the stability of the edge against $N_{\max}$ is a consequence of the existence of the phase transition, and information on the phase transition is lost with too small $N_{\max}$.

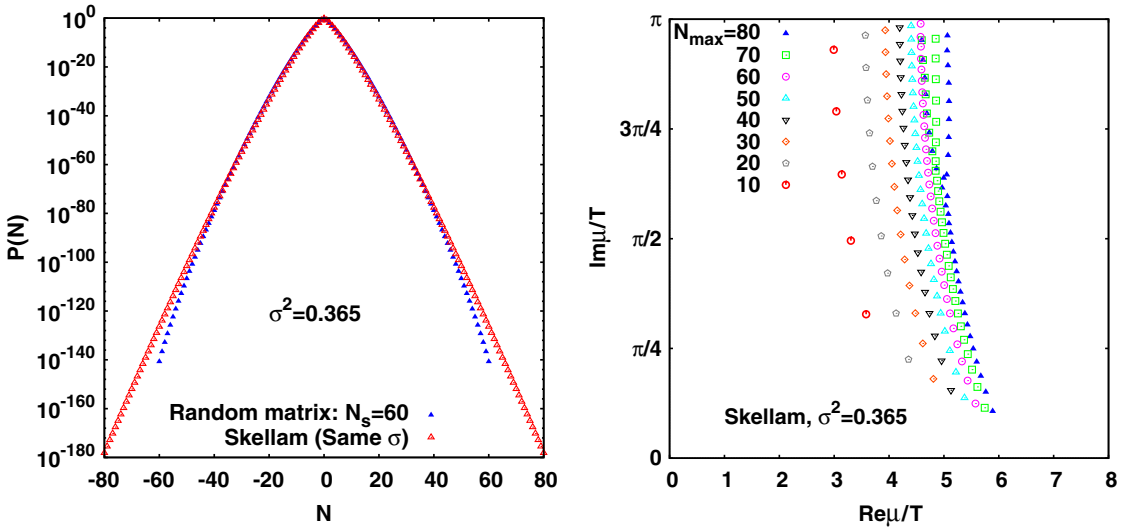

FIG. 8 (color online). Left: $P(N)$ for the random matrix model at $T = T_c$ and $m = 0.05$, and the corresponding Skellam distribution. Right: Distribution of Lee-Yang zeros for a truncated Skellam partition function.

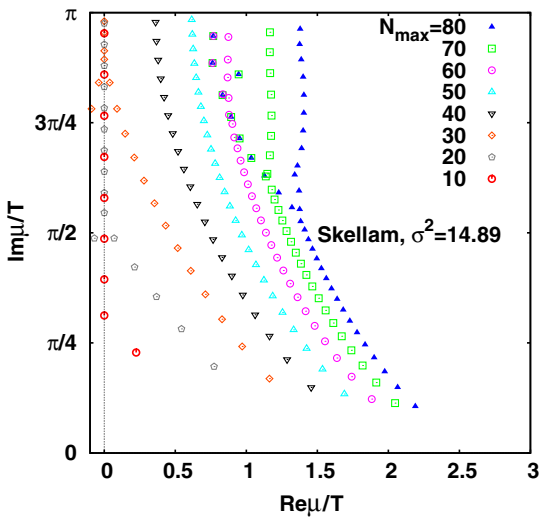

FIG. 9 (color online). Distribution of the zeros for the Skellam partition function for $\sigma^2 = 14.89$.

V. DISCUSSION

A. Comparison with $N_{\max}$ for cumulants

In the previous section, we have shown that the edge of the distribution of the Yang-Lee zeros remains unchanged when the tail part of the canonical partition function is missing. In practice, this property gives implications for necessary statistics in heavy ion studies of the net-baryon number fluctuations and in lattice QCD calculations. Since the sufficient $N_{\max}$ to see the stable edge depends on the system volume, here we compare it with the corresponding $N_{\max}^{(i)}$ for the ith-order cumulants. We consider only even-order ones for the net-baryon number at $\mu = 0$ since we are looking at $Z(T, V, N)$ rather than $P(N)$ which becomes asymmetric with respect to N at $\mu > 0$. Thus, the first central moment $\delta N = N - \langle N \rangle = N$. The second-, fourth-, and sixth-order cumulants c_n $(n = 2, 4, 6)$ read

$$c_2 = \langle (\delta N)^2 \rangle, \tag{35}$$

$$c_4 = \langle (\delta N)^4 \rangle - 3\langle (\delta N)^2 \rangle^2, \tag{36}$$

$$c_6 = \langle (\delta N)^6 \rangle - 15\langle (\delta N)^4 \rangle \langle (\delta N)^2 \rangle + 30\langle (\delta N)^2 \rangle^3. \tag{37}$$

The property of the higher-order cumulants of the net-baryon number probability distribution for changing $N_{\max}$ was studied in Ref. [42] by using a chiral quark-meson model. For sufficiently large volume, it was shown that $N_{\max}^{(i)}$ for the cumulants approximately scales with $\sqrt{V}$.

We summarize the values of each $N_{\max}$ in Table I. The calculations are done for $T = T_c$ and $m = 0.05$ in the random matrix model. Owing to the narrow $Z(N)$, even the sixth-order cumulant for $N_s = 100$ only requires $N_{\max}^{(6)} = 7$, i.e, $-7 \le N \le 7$ to reconstruct it from $Z(T, V, N)$, while the edge of the Yang-Lee zeros demands $N_{\max} = 21$. The small $N_{\max}^{(6)}$ implies the system volume is

TABLE I. $N_{\max}$ necessary for reconstructing the ith-order cumulants and edge of the Yang-Lee zeros from $Z(N)$ in the random matrix model at $T = T_c$ and $m = 0.05$.

N_s	$N_{\max}^{(2)}$	$N_{\max}^{(4)}$	$N_{\max}^{(6)}$	$N_{\max}$
60	3	4	6	21
80	3	5	6	26
100	4	5	7	30

not large enough to exhibit the $\sqrt{V}$ scaling regime of the cumulants. This can be understood from the small value of σ^2 in the random matrix model calculations. The rapid decay of $P(N)$ gives a rather weak dependence of $N_{\max}$ for the higher-order cumulants. For a sufficiently large volume, one expects that $P(N)$ resembles Gaussian near the peak, while the probability distribution (Fig. 8) has a sharp peak. Thus, we cannot assess the value of $N_{\max}$ needed in a realistic situation relevant for heavy ion collisions. Moreover, the baryon number carried in this model is not a physical one, as mentioned above. All we can say is that one may need more statistics than with higher-order cumulants.

B. Skellam distribution for large volume

In the fluctuation measurements at RHIC, the observed $P(N)$ can be well described by the Skellam distribution and the deviation from the Skellam distribution existing in the tail results in higher-order cumulants different from the Skellam case. The obtained variance reaches $\sigma^2 \sim 10$ [16,72] at the most central bin. Thus, it is instructive to give a reference for the distribution of the spurious Yang-Lee zeros based on the Skellam distribution. Here we pick up the data for $\sqrt{s_{NN}} = 7.7$ GeV at the most central bin, which gives $\sigma^2 = 14.89$ and $M = 14.41$ with the available bin from $N = 0$ to $N = 34$.[5] As mentioned in Sec. II, one can construct $Z(N)$ from $-34 \le N \le 34$ according to charge conjugation symmetry [46]. In the Skellam distribution for $\sigma^2 = 14.89$, we find that $N_{\max}^{(i)} = 13$, 20 and 26 for the second-, fourth-, and sixth-order cumulants, respectively. Note that these $N_{\max}^{(i)}$ apply to the cumulants at $\mu = 0$. The data do not have enough statistics for the sixth-order cumulant at freeze-out μ.

We plot the distribution of the Yang-Lee zeros for the constructed Skellam distribution with $\sigma^2 = 14.89$ in Fig. 9. The basic feature is the same as the small σ^2 case (Fig. 8). The line of zeros moves toward infinity as $N_{\max}$ increases. One sees that some zeros below $N = 30$ appear on the imaginary μ axis, which corresponds to the unit circle in the complex fugacity plane. This means that for a large volume case, the zeros can appear on the imaginary axis when the tail of the $Z(N)$ is not provided. In the Skellam distribution, these zeros can be obtained directly by looking at the truncated partition function on the imaginary μ axis, for $\lambda = e^{i\theta}$,

$$\mathcal{Z}^{\mathrm{tr}}_{\mathrm{Skellam}}(\theta) = 2 \sum_{N=-N_{\max}}^{N_{\max}} I_N(\sigma^2) \cos N\theta, \qquad (38)$$

which converges into Eq. (34) with oscillations giving zeros on imaginary μ.

[5]The data for $N = 0$ and $N = 34$ have only one event.

VI. CONCLUDING REMARKS

In this paper, we present analyses of partition function zeros which can be obtained from a truncated series of the fugacity expansion. By solving an extended chiral random matrix model which has a periodicity in the imaginary chemical potential, we compare the exact location of the Yang-Lee zeros and those obtained from the truncated series. We find that the edge of the distribution of the zeros is insensitive to the truncation of higher-order terms in the fugacity expansion to some degree. We find a similar behavior in lattice QCD at high temperature in the context of the Roberge-Weiss phase transition. This observation indicates that those higher-order terms may have limited influences in the search of the location of the phase boundary in lattice QCD calculations and heavy ion experiments. Although the distribution of zeros exists in systems without phase transition, due to the truncation, the zeros closest to the real μ axis are stable against truncation if the system has a phase transition or crossover. The spurious zeros in the Skellam distribution move toward infinity against the truncation. Therefore, one can distinguish whether or not the distribution is related to the phase transition by looking at the stability of the edge of the distribution against the truncation.

Although the information on the Stokes boundary is lost in the case of too small $N_{\max}$, we expect that it does not mean that all the relevant information on the phase transition gets lost in the truncated partition function. This expectation follows from the fact that the sixth- and higher-order cumulants at $\mu = 0$ should be influenced by the phase transition and the truncated series is still able to reproduce them. It would be interesting to see how the distribution of the zeros in the small $N_{\max}$ cases in Figs. 5–6 is related to the remnant of the phase transition.

The order of the truncation in the fugacity series to obtain the stable edge of the Yang-Lee zeros, $N_{\max}$, is nevertheless found to be much larger than those for higher-order cumulants. We cannot make a quantitative assessment on realistic values for heavy ion experiments due to the lack of connection between the model and the real world. We hope that such an estimate becomes feasible in the near future.

ACKNOWLEDGMENTS

The authors would like to thank X. Luo and N. Xu for providing the numerical data of the STAR Collaboration. They would like to gratefully acknowledge B. Friman and K. Redlich for fruitful discussion and continuous encouragement. They acknowledge stimulating discussions with Ph. de Forcrand, F. Karsch, J. Knoll, V. Koch, K. Nagata, and J. Wambach. This work was supported by the Grants-in-Aid for Scientific Research on Innovative Areas from MEXT (No. 24105008), the Grants-in-Aid for Scientific Research from JSPS (No. 15H03663 and No. 26610072),

HIC for FAIR, and the Polish Science Foundation (NCN), under Maestro Grant No. 2013/10/A/ST2/00106.

APPENDIX A: DERIVATION OF THE CANONICAL PARTITION FUNCTION IN A CHIRAL RANDOM MATRIX MODEL

In the following, we derive an analytic expression for $Z(T,N_s,N)$ from Eq. (28). First we rewrite the μ-dependent part in terms of the fugacity $\lambda = e^{\mu/T}$.

Since

$$\mathrm{Re}\left[\left(A\sinh\frac{\mu}{2T}+i\right)^{2k_1}\left(A\sinh\frac{\mu}{2T}-i\right)^{2k_2}\right] \tag{A1}$$

$$=\left(A^2\sinh^2\frac{\mu}{2T}+1\right)^{k_1+k_2}\cos[2(k_1-k_2)\phi], \tag{A2}$$

where

$$\tan\phi=\left(A\sinh\frac{\mu}{2T}\right)^{-1}, \tag{A3}$$

and the imaginary part vanishes after summation over k_1 and k_2, using the Chebychev polynomial

$$T_{k_1-k_2}(\cos 2\phi)=\cos[2(k_1-k_2)\phi] \tag{A4}$$

and

$$\cos 2\phi=\left(A^2\sinh\frac{\mu}{2T}-1\right)/\left(A^2\sinh\frac{\mu}{2T}+1\right), \tag{A5}$$

we have the partition function $\mathcal{Z}$ as

$$\begin{aligned}\mathcal{Z}=&\sum_{k_1,k_2=0}^{N_s/2}\binom{N_s/2}{k_1}\binom{N_s/2}{k_2}(N_s-k_1-k_2)!\\&\times{}_1F_1(k_1+k_2-N_s;1;-m^2N_s)(-N_s\tilde{T}^2A^2/4)^{k_1+k_2}\\&\times\left(\lambda+\frac{1}{\lambda}+\frac{2(2-A^2)}{A^2}\right)^{k_1+k_2}\\&\times T_{k_1-k_2}\left(\frac{\lambda+\lambda^{-1}-2(A^2+2)/A^2}{\lambda+\lambda^{-1}-2(A^2-2)/A^2}\right).\end{aligned} \tag{A6}$$

Expanding the Chebychev polynomial by the following expression,

$$T_n(x)=\begin{cases}1 & n=0\\ n\sum_{k=0}^{n}(-2)^k\frac{(n+k-1)!}{(n-k)!(2k)!}(1-x)^k & n\geq 1,\end{cases} \tag{A7}$$

and using binomial expansion in the third line of (A6), we can express $\mathcal{Z}$ in terms of $\lambda+\lambda^{-1}$. We obtain Eq. (29) by applying the projection (6). Note that the maximum power of λ is given by N_s.

APPENDIX B: ROBERGE-WEISS TRANSITION AS A THERMAL CUT

In this appendix, we give a brief explanation of the cut arising from the Fermi distribution function and apply it to the Roberge-Weiss transition in QCD.

1. Thermal cut in free Fermi gas

The thermodynamic potential of the free Fermi gas is given by

$$\Omega_f\sim-\int\frac{d^3p}{(2\pi)^3}\ln[1+e^{-\beta(E_p-\mu)}]+(\mu\to-\mu), \tag{B1}$$

where $E_p=\sqrt{p^2+m^2}$. When the chemical potential μ has an imaginary part, $\mu_I=\theta T$, the imaginary part gives a phase in front of the Boltzmann factor,

$$1+e^{-\beta(E_p-\mu)}=1+e^{i\theta}e^{-\beta(E_p-\mu_R)}, \tag{B2}$$

where $\mu=\mu_R+i\mu_I$. Therefore, for $\theta=\pm\pi$, the phase gives -1 and the thermodynamic potential has a logarithmic cut at $\theta=\pm\pi$ and $m\leq\mu_R<\infty$. The antiparticle term also gives the cut symmetric with respect to the imaginary axis. In Ref. [73], it is pointed out that the branch point singularity limits the convergence radius when one tries to analytically continue the results in the imaginary chemical potential to the real one. Since this cut originates from the Fermi distribution, the same analytic structure appears in chiral models with fermions [69].

2. Roberge-Weiss transition

In QCD at high temperature, quarks are deconfined and have a light mass owing to chiral restoration. Since the deconfinement can be expressed as a breaking of $Z(N_c)$ symmetry, it is useful to resort to chiral effective models with the Polyakov loop background [74–76] which successfully describe the Roberge-Weiss transition [64,65,77]. Then, the relevant leading single-quark contribution to the thermodynamic potential reads

$$\begin{aligned}\Omega_{q\bar{q}}\sim&-\int\frac{d^3p}{(2\pi)^3}\ln[1+3\Phi e^{-\beta(E_p-\mu_q)}]\\&+(\mu_q\to-\mu_q,\Phi\to\bar{\Phi}),\end{aligned} \tag{B3}$$

where $\mu_q=\mu/3$ is the quark chemical potential and Φ is the expectation value of the Polyakov loop. For the antiquark contribution, the conjugate $\bar{\Phi}$ couples to the thermal distribution. At the imaginary chemical potential, the Polyakov loop Φ acquires a complex phase φ. One may express $\Phi=|\Phi|e^{i\varphi}$. Then the thermodynamic contribution becomes

$$1 + 3\Phi e^{-\beta(E_p-\mu_q)} = 1 + 3|\Phi|e^{i(\varphi-\theta_q)}e^{-\beta(E_q-\mu_{q,R})}. \quad \text{(B4)}$$

The phase of the Polyakov loop φ varies as a function of the imaginary quark chemical potential θ_q. The Roberge-Weiss transition at $\theta_q = \pi/3$ can be understood as a transition from one $Z(3)$ sector with $\varphi = 0$ to another one $\varphi = -2\pi/3$ [65]. Then the coupling between φ and θ_q gives the prefactor -1 in front of the Boltzmann factor. Moreover, $|\Phi| \sim 1$ in the deconfined phase and the prefactor 3 allow this function to have the singularity at $\mu_{q,R} = 0$. This feature gives the cut drawn as the RW transition line in Fig. 7. A derivation based on the Gaussian $P(N)$ can be found in Ref. [55]. In the confinement phase where $|\Phi| \sim 0$, this term is suppressed, and the thermal cut from the quark does not appear.

[1] Y. Aoki, G. Endrődi, Z. Fodor, S. D. Katz, and K. K. Szabó, The order of the quantum chromodynamics transition predicted by the standard model of particle physics, Nature (London) **443**, 675 (2006).

[2] S. Muroya, A. Nakamura, C. Nonaka, and T. Takaishi, Lattice QCD at finite density—An introductory review, Prog. Theor. Phys. **110**, 615 (2003).

[3] P. de Forcrand, Simulating QCD at finite density, *Proc. Sci.*, LAT2009 (2009) 010.

[4] K. Fukushima and T. Hatsuda, The phase diagram of dense QCD, Rep. Prog. Phys. **74**, 014001 (2011).

[5] K. Fukushima and C. Sasaki, The phase diagram of nuclear and quark matter at high baryon density, Prog. Part. Nucl. Phys. **72**, 99 (2013).

[6] M. Asakawa and K. Yazaki, Chiral restoration at finite density and temperature, Nucl. Phys. **A504**, 668 (1989).

[7] M. Stephanov, QCD phase diagram and the critical point, Prog. Theor. Phys. Suppl. **153**, 139 (2004).

[8] N. Xu (STAR Collaboration), An overview of STAR experimental results, Nucl. Phys. **A931**, 1 (2014).

[9] R. A. Soltz (PHENIX Collaboration), PHENIX bean energy scan results, Nucl. Phys. **A931**, 780 (2014).

[10] M. Stephanov, K. Rajagopal, and E. Shuryak, Signatures of the tricritical point in QCD, Phys. Rev. Lett. **81**, 4816 (1998).

[11] M. Stephanov, K. Rajagopal, and E. Shuryak, Event-by-event fluctuations in heavy ion collisions and the QCD critical point, Phys. Rev. D **60**, 114028 (1999).

[12] M. Asakawa, U. W. Heinz, and B. Müller, Fluctuation probes of quark deconfinement, Phys. Rev. Lett. **85**, 2072 (2000).

[13] S. Jeon and V. Koch, Charged particle ratio fluctuation as a signal for QGP, Phys. Rev. Lett. **85**, 2076 (2000).

[14] Y. Hatta and M. A. Stephanov, Proton-number fluctuation as a signal of the QCD critical end point, Phys. Rev. Lett. **91**, 102003 (2003).

[15] M. M. Aggarwal *et al.* (STAR Collaboration), Higher moments of net proton multiplicity distributions at RHIC, Phys. Rev. Lett. **105**, 022302 (2010).

[16] L. Adamczyk *et al.* (STAR Collaboration), Energy dependence of moments of net-proton multiplicity distributions at RHIC, Phys. Rev. Lett. **112**, 032302 (2014).

[17] L. Adamczyk *et al.* (STAR Collaboration), Beam energy dependence of moments of the net-charge multiplicity distributions in Au + Au collisions at RHIC, Phys. Rev. Lett. **113**, 092301 (2014).

[18] P. Braun-Munzinger, K. Redlich, and J. Stachel, Particle production in heavy ion collisions, in *Quark-Gluon Plasma 3*, edited by R. C. Hwa and X. N. Wang (World Scientific, Singapore, 2004), p. 491.

[19] A. Andronic, P. Braun-Munzinger, and J. Stachel, Hadron production in central nucleus-nucleus collisions at chemical freeze-out, Nucl. Phys. **A772**, 167 (2006).

[20] J. Cleymans, H. Oeschler, K. Redlich, and S. Wheaton, Comparison of chemical freeze-out criteria in heavy-ion collisions, Phys. Rev. C **73**, 034905 (2006).

[21] C. R. Allton, M. Döring, S. Ejiri, S. J. Hands, O. Kaczmarek, F. Karsch, E. Laermann, and K. Redlich, Thermodynamics of two flavor QCD to sixth order in quark chemical potential, Phys. Rev. D **71**, 054508 (2005).

[22] O. Kaczmarek, F. Karsch, E. Laermann, C. Miao, S. Mukherjee, P. Petreczky, C. Schmidt, W. Soeldner, and W. Unger, Phase boundary for the chiral transition in $(2 + 1)$-flavor QCD at small values of the chemical potential, Phys. Rev. D **83**, 014504 (2011).

[23] F. Karsch and K. Redlich, Probing freeze-out condition in heavy ion collisions with moments of charge fluctuations, Phys. Lett. B **695**, 136 (2011).

[24] B. Friman, F. Karsch, K. Redlich, and V. Skokov, Fluctuations as probe of the QCD phase transition and freeze-out in heavy ion collisions at LHC and RHIC, Eur. Phys. J. C **71**, 1694 (2011).

[25] K. Morita, B. Friman, and K. Redlich, Criticality the net-baryon number probability distribution at finite density, Phys. Lett. B **741**, 178 (2015).

[26] Y. Hatta and Y. Ikeda, Universality, the QCD critical and tricritical point, and the quark number susceptibility, Phys. Rev. D **67**, 014028 (2003).

[27] V. Koch, Hadronic fluctuations and correlations, arXiv: 0810.2520.

[28] M. A. Stephanov, Non-Gaussian Fluctuations near the QCD Critical Point, Phys. Rev. Lett. **102**, 032301 (2009).

[29] S. Aoki, H. Fukaya, and Y. Taniguchi, Chiral symmetry restoration, the eigenvalue density of the Dirac operator, and the axial $U(1)$ anomaly at finite temperature, Phys. Rev. D **86**, 114512 (2012).

[30] T. Bhattacharya, M. I. Buchoff, N. H. Christ, H. T. Ding, R. Gupta, C. Jung, F. Karsch, Z. Lin, R. D. Mawhinney,

G. McGlynn, S. Mukherjee, D. Murphy, P. Petreczky, D. Renfrew, C. Schroeder, R. A. Soltz, P. M. Vranas, and H. Yin, QCD phase transition with chiral quarks and physical quark masses, Phys. Rev. Lett. **113**, 082001 (2014).

[31] S. Ejiri, F. Karsch, E. Laermann, C. Miao, S. Mukherjee, P. Petreczky, C. Schmidt, W. Soeldner, and W. Unger, Magnetic equation of state in $(2+1)$-flavor QCD, Phys. Rev. D **80**, 094505 (2009).

[32] R. D. Pisarski and F. Wilczek, Remarks on the chiral transition in chromodynamics, Phys. Rev. D **29**, 338 (1984).

[33] J. Engels and F. Karsch, Scaling functions of the free energy density and its derivatives for the $3d$ $O(4)$ model, Phys. Rev. D **85**, 094506 (2012).

[34] C. Sasaki, B. Friman, and K. Redlich, Quark number fluctuations in a chiral model at finite baryon chemical potential, Phys. Rev. D **75**, 054026 (2007).

[35] C. Sasaki, B. Friman, and K. Redlich, Susceptibilities and the phase structure of a chiral model with Polyakov loops, Phys. Rev. D **75**, 074013 (2007).

[36] S. Floerchinger and C. Wetterich, Chemical freeze-out in heavy ion collisions at large baryon densities, Nucl. Phys. **A890-891**, 11 (2012).

[37] K. Fukushima, Hadron resonance gas and mean-field nuclear matter for baryon number fluctuations, Phys. Rev. C **91**, 044910 (2015).

[38] M. Asakawa, S. Ejiri, and M. Kitazawa, Third moments of conserved charges as probes of QCD phase structure, Phys. Rev. Lett. **103**, 262301 (2009).

[39] M. A. Stephanov, Sign of kurtosis near the QCD critical point, Phys. Rev. Lett. **107**, 052301 (2011).

[40] V. Skokov, B. Friman, and K. Redlich, Quark number fluctuations in the Polyakov loop-extended quark-meson model at finite baryon density, Phys. Rev. C **83**, 054904 (2011).

[41] K. Morita, V. Skokov, B. Friman, and K. Redlich, Net baryon number probability distribution near chiral phase transition, Eur. Phys. J. C **74**, 2706 (2014).

[42] K. Morita, B. Friman, K. Redlich, and V. Skokov, Net quark number probability distribution near the chiral crossover transition, Phys. Rev. C **88**, 034903 (2013).

[43] A. Hasenfratz and D. Toussaint, Canonical ensembles and nonzero density quantum chromodynamics, Nucl. Phys. **B371**, 539 (1992).

[44] R. Fukuda, A. Nakamura, and S. Oka, Canonical approach to finite density QCD with multiple precision computation, arXiv:1504.06351.

[45] A. Nakamura, S. Oka, and Y. Taniguchi, Canonical approach to finite density QCD with winding number expansion, *Proc. Sci.*, LATTICE2015 (2015) 198.

[46] A. Nakamura and K. Nagata, Probing QCD phase structure by baryon multiplicity distribution, arXiv:1305.0760.

[47] C. N. Yang and T. D. Lee, Statistical theory of equations of state and phase transitions. I. Theory of condensation, Phys. Rev. **87**, 404 (1952).

[48] T. D. Lee and C. N. Yang, Statistical theory of equations of state and phase transitions. II. Lattice gas and Ising model, Phys. Rev. **87**, 410 (1952).

[49] R. A. Blythe and M. R. Evans, The Lee-Yang theory of equilibrium and nonequilibrium phase transitions, Braz. J. Phys. **33**, 464 (2003).

[50] I. Bena, M. Droz, and A. Lipowski, Statistical mechanics of equilibrium and nonequilibrium phase transitions: The Yang-Lee formalism, Int. J. Mod. Phys. B **19**, 4269 (2005).

[51] P. J. Kortmann and R. B. Griffiths, Density of Zeros on the Lee-Yang Circle for Two Ising Ferromagnets, Phys. Rev. Lett. **27**, 1439 (1971).

[52] M. E. Fisher, Yang-Lee Edge Singularity and ϕ^3 Field Theory, Phys. Rev. Lett. **40**, 1610 (1978).

[53] S. Ejiri, Y. Shinno, and H. Yoneyama, Complex singularities around QCD critical point at finite densities, Prog. Theor. Exp. Phys. **2014**, 083B02 (2014).

[54] K. Nagata, S. Motoki, Y. Nakagawa, A. Nakamura, and T. Saito (XQCD-J Collaboration), Towards extremely dense matter on the lattice, Prog. Theor. Exp. Phys. **2012**, 01A103 (2012).

[55] K. Nagata, K. Kashiwa, A. Nakamura, and S. M. Nishigaki, Lee-Yang zero distribution of high temperature QCD and Roberge-Weiss phase transition, Phys. Rev. D **91**, 094507 (2015).

[56] M. Kitazawa and M. Asakawa, Revealing baryon number fluctuations from proton number fluctuations in relativistic heavy ion collisions, Phys. Rev. C **85**, 021901 (2012).

[57] K. Nagata and A. Nakamura, EoS of finite density QCD with Wilson fermisions by multi-parameter reweighting and Taylor expansion, J. High Energy Phys. 04 (2012) 092.

[58] M. Stephanov, QCD critical point and complex chemical potential singularities, Phys. Rev. D **73**, 094508 (2006).

[59] M. A. Halasz, A. D. Jackson, R. E. Shrock, M. A. Stephanov, and J. J. M. Verbaarschot, Phase diagram of QCD, Phys. Rev. D **58**, 096007 (1998).

[60] P. de Forcrand and O. Philipsen, The QCD phase transition for small densities from imaginary chemical potential, Nucl. Phys. **B642**, 290 (2002).

[61] P. de Forcrand and O. Philipsen, The chiral critical line of $n_f = 2+1$ QCD at zero and non-zero baryon density, J. High Energy Phys. 01 (2007) 077.

[62] M. D'Elia and M. P. Lombardo, Finite density QCD via an imaginary chemical potential, Phys. Rev. D **67**, 014505 (2003).

[63] J. B. Kogut and M. A. Stephanov, *The Phases of Quantum Chromodynamics: From Confinenment to Extreme Environments* (Cambridge University Press, Cambridge, England, 2004).

[64] Y. Sakai, K. Kashiwa, H. Kouno, and M. Yahiro, Polyakov loop extended Nambu-Jona-Lasinio model with imaginary chemical potential, Phys. Rev. D **77**, 051901(R) (2008).

[65] K. Morita, V. Skokov, B. Friman, and K. Redlich, Probing deconfinement in a chiral effective model with Polyakov loop at imaginary chemical potential, Phys. Rev. D **84**, 076009 (2011).

[66] A. Roberge and N. Weiss, Gauge theories with imaginary chemical potential and the phases of QCD, Nucl. Phys. **B275**, 734 (1986).

[67] M. A. Halasz, A. D. Jackson, and J. J. M. Verbaarschot, Yang-Lee zeros of a random matrix model for QCD at finite density, Phys. Lett. B **395**, 293 (1997).

[68] D. M. Smith, Fortran Software for Multiple Precision, http://myweb.lmu.edu/dmsmith/FMLIB.html.

[69] V. Skokov, K. Morita, and B. Friman, Mapping out the phase diagram of strongly interacting matter, Phys. Rev. D **83**, 071502(R) (2011).

[70] B. Friman, Phase transitions at finite density, Acta Phys. Pol. B **5**, 707 (2012).
[71] J. G. Skellam, The frequency distribution of the difference between two poisson variates belonging to different populations, Journal of the Royal Statistical Society Series A (General) **109**, 296 (1946).
[72] P. Braun-Munzinger, B. Friman, F. Karsch, K. Redlich, and V. Skokov, Net-proton probability distribution in heavy ion collisions, Phys. Rev. C **84**, 064911 (2011).
[73] F. Karbstein and M. Thies, How to get from imaginary to real chemical potential, Phys. Rev. D **75**, 025003 (2007).
[74] K. Fukushima, Chiral effective model with the Polyakov loop, Phys. Lett. B **591**, 277 (2004).
[75] C. Ratti, M. A. Thaler, and W. Weise, Phases of QCD: Lattice thermodynamics and a field theoretical model, Phys. Rev. D **73**, 014019 (2006).
[76] B. J. Schaefer, M. Wagner, and J. Wambach, Thermodynamics of $(2+1)$-flavor QCD: confronting models with lattice studies, Phys. Rev. D **81**, 074013 (2010).
[77] K. Morita, V. Skokov, B. Friman, and K. Redlich, Role of mesonic fluctuations in the Polyakov loop extended quark-meson model at imaginary chemical potential, Phys. Rev. D **84**, 074020 (2011).